Response to Reviewer #2

Dear reviewer,
Please find below our answers to the constructive remarks you raised regarding our manuscript below. They all have been carefully considered and will provide what we feel is a much improved manuscript. You will also find, below, all of the modified figures of the new manuscript and Supplementary Material, below.

Comment #1 (C1): *The structure of the manuscript needs some improvement. While the first part (Introduction, Material and Methods) are very well written (although lacking some details about age-model), the discussion relative to the model outputs is not so clear. I find the discussion about model output section very difficult to follow, needs to be simplified in order to improve the understanding and to be better integrated with the proxy data, not to be discussed separately.*

Reply #1 (R1): We agree with Reviewer #2. Therefore, we revised the structure of our manuscript, based (as well) on Reviewer #1' suggestions. An entire chapter is now devoted to the results. In the discussion, empirical data and model outputs are interpreted simultaneously in chapter 5. Particularly, sections 5.1 to 5.3 discuss PP patterns regarding the LGM, the deglaciation, and the Holocene, respectively. We believe that this new structure is helpful to build a more coherent scheme behind PP variability.

Below is the new structure of chapters 4 and 5:
4. Results
4.1. Coccolith abundances and reconstructed primary productivity over the last 26 kyrs
4.2. Simulated primary productivity and physicochemical profiles in the northeastern Bay of Bengal
5. Forcing factors behind PP variations over the last 26 kyrs: the inputs of model-data comparisons
5.1. During the glacial period
5.2. During the last deglaciation
5.3. During the Holocene

In detail:

- In section 4.1, we present and describe coccolith species abundances and reconstructed PP (Figure 1 of Author Reponse (Fig. AC1)).
- Section 4.2. relies on new IPSL-CM5A-LR figures dedicated to model results, that help understanding and improving model output interpretations i.e. i) simulated PP maps (Fig. AC2), and ii) simulated vertical profiles of potential temperature, salinity, potential density, and nitrate content of the northeastern Bay of Bengal under four experimental runs (Fig. AC3), that help discussing climate conditions for the LGM (LGMc), the Heinrich Stadial 1 (LGMf), and the Mid-Holocene (MH), compared to preindustrial (CTRL). We show the results of annual mean, summer seasons mean (from June to August, JJA) and winter seasons mean (from December to February) for all these specific time intervals, in order to evaluate PP changes during the monsoonal seasons.

- In sections 5.1 to 5.3, we compare our reconstructed PP signal with the published empirical records previously documented in Fig. AC4, and with TraCE-21 transient simulations of the upper water column stratification, SSS, SST and net precipitation (P-E), previously documented in Fig. 5. Merging our previous Figures 4 and 5 into a new figure (Fig. AC4), allows to better discuss PP variations in the monsoonal context. We also combine atmospheric and oceanic outputs of the four experiments run together with the simulated PP obtained by the IPSL-CM5A-LR model in order to better discuss and interpret our reconstructed PP during the last glacial period (section 5.1; Fig, AC5, AC6), the last deglaciation (section 5.2; Fig. AC7, AC8) and the Holocene (section 5.3; Fig, AC9).

***C2:** The figure 2 is not very useful, it repeats data that are shown later in other figures several times. For example, showing the d18Osw and the GISP2 ice-core d18O is not really relevant, as we see the proxy data already tuned to the ice-core data. I assume that Marzin et al., (2013) contains a plot showing this, so these two curves are not needed here. An important point regarding the age-model is that if, despite the large number of radiocarbon ages, the proxy data is tuned to the GISP ice-core d18O, later comparisons between proxy and ice-core data are not very well sustained (circularity). The authors should keep this in mind when discussing about it at L. 205-207.*

R2: The initial Figure 2 does not exist anymore. GISP $\delta^{18}O$ and $\delta^{18}O_{G.ruber}$ obtained on core MD77-169 are now only evoked when dealing with the age model (Figure S1). *Florisphaera profunda* distribution and PP reconstructions are presented within the a new figure (Fig. AC1), that is entirely devoted to micropalaeontological results (i.e. abundances of *F. profunda, Gephyrocapsa* spp. and *Emiliania huxleyi* together with PP estimates).

We thank Reviewer # 2 for highlighting that our phrasing in lines 205-207 could be seen as a circular reasoning, since proxy data are in part tuned to the GISP $\delta^{18}O$ signal. However, our micropalaeontological data are well in phase with numerous geochemical data obtained elsewhere in the Tropical Indian Ocean and the Chinese continent, based on sediment cores and speleothems with totally independent age models. They also match very well the TraCE 21 and IPSL-CM5A-LR outputs obtained here. Such feature, together with its use in previous works (Marzin et al., 2013; Yu et al., 2017; Ma et al., 2019), point to a robust age model and demonstrate that our micropalaeontological data can be discussed properly in the light of the rapid climatic changes recorded in northern high-latitudes. To avoid any confusion, we rephrased lines 205-207 of the manuscript focusing on the relationship that exists between PP and SSS.

***C3:** I find particularly intriguing the change in the salinity-PP relationship before and after LGM (L. 213-222).. The authors suggest that the higher PP during low salinity between 26-19ka are due to higher wind mixing. Are there independent proxy evidence of this coupling? For example, loess deposits that could record changes in wind intensity which could support their view? And why the wind-forcing gets weaker after the LGM?*

R3: To our knowledge, there is a high-resolution record of loess grain size from the northeastern China which indicates the local winter wind intensity (Sun et al., 2012; Zhang et al., 2016). The record shows that the winter wind is stronger during LGM than during the late Holocene. However, there is no published record of wind intensity for the Bay Bengal and Andaman Sea. We think it might be questionable to use the wind record over the northwestern China to interpret the Bay of Bengal as these two regions are not close to one another and the wind directions are different (Fig. 1c; Sun et al., 2012). We checked the modeling outputs and found that compared to preindustrial (CTRL), stronger summer winds and weaker winter winds prevailed over annually saltier sea surface in the Bay of Bengal during the LGM (Fig. AC5, AC6). This implies that the winter wind over the northwestern China and the Bay of Bengal are not strengthened at the same period during the LGM. Therefore, we think if wind-mixing is stronger over the Bay of Bengal during the LGM, it should be related to strengthened summer winds. However, the relationship between PP and SSS of MD77-176 encourages us to explore further mechanisms behind PP (and SSS) variability at that time. We have also found that IPSL-CM5A-LR outputs show spatial differences of SSS in the Bay of Bengal, and particularly, that the studied area could have been associated to low SSS during the LGM (Sijinkumar et al. (2016). Our best explanation is that during the LGM, i.e. under relatively low sea-level, and a more proximal environment for MD77-176, PP and SSS react to the Irrawaddy dynamic in the same way as proximal environment do, today (Fig. 1). Indeed, higher (lower) nutrient and freshwater inputs from the Irrawaddy river, may trigger higher PP and lower SSS, and vice versa. Such assumption is confirmed in Fig. AC2 and AC3 where PP strongly increases (Fig. AC2), when vertical profiles clearly depict a change from open ocean type to coastal one (Fig. AC3). Our scenario seems therefore to provide a suitable explanation behind the PP pattern reconstructed for the LGM.

Bearing in mind that the LGMc experiment of IPSL-CM5A-LR gives us a mean state of PP and SSS conditions and may not simulate the high-resolution PP changes discussed here, we only evoke the possible Irrawaddy river influence on PP distribution during the LGM, with caution.

***C4:** Finally, in the section Data availability the authors indicate that "Data to this paper can be required. Please contact the X. Zhou or S. Duchamp-Alphonse.". Copernicus journals (including Climate of the Past) have a very clear policy regarding data curation (https://www.climate-of-the-past.net/about/data_policy.html), which "requests depositing data that correspond to journal articles in reliable (public) data repositories, assigning digital object identifiers, and properly citing data sets as individual contributions". Clearly the current statement about data availability does not meet this criteria, and all data and code should be archive somewhere or included as supplementary material.*

R4: Thanks for this reminding. We have added our data in the supplementary materials.

***C5:** Some minor corrections: L. 104. Abbreviate Arabian Sea L. 177. Strange symbol between longitude and latitude.*

R5: We have corrected them.

***C6:** Fig. 1f, why choosing SON instead of JJA as the other panels?*

R6: Because the occupation of the input fresh water is the largest during SON in the northeastern Indian Ocean at modern time, lagging the maximum precipitation over the South Asia.

R7: modified supplementary figures are Fig. AC10 to AC15

References

Marzin et al., 2013. Glacial fluctuations of the Indian monsoon and their relationship with North Atlantic climate: new data and modeling experiments, Climate of the Past, 9, 2135–2151.

Yu et al., 2018. Antarctic Intermediate Water penetration into the Northern Indian Ocean during the last deglaciation. Earth and Planetary Science Letters, 500, 67–75.

Ma et al., 2019. Changes in Intermediate Circulation in the Bay of Bengal since the Last Glacial Maximum as inferred from benthic foraminifera assemblages and geochemical proxies. Geochemistry, Geophysics, Geosystems, 20, 1592-1608.

Sijinkumar et al., 2016. δ18O and salinity variability from the Last Glacial Maximum to Recent un the Bay of Bengal and Andaman Sea. Quaternary Science Reviews, 135, 79–91.

Sun et al., 2012. Influence of Atlantic meridional overturning circulation on the East Asian winter monsoon. Nature Geoscience, 5, 46-49.

Zhang et al., 2016. Dynamics of primary productivity in the northern South China Sea over the past 24,000 years. Geochemistry, Geophysics, Geosystems, 17, 4878-4891.

Figures

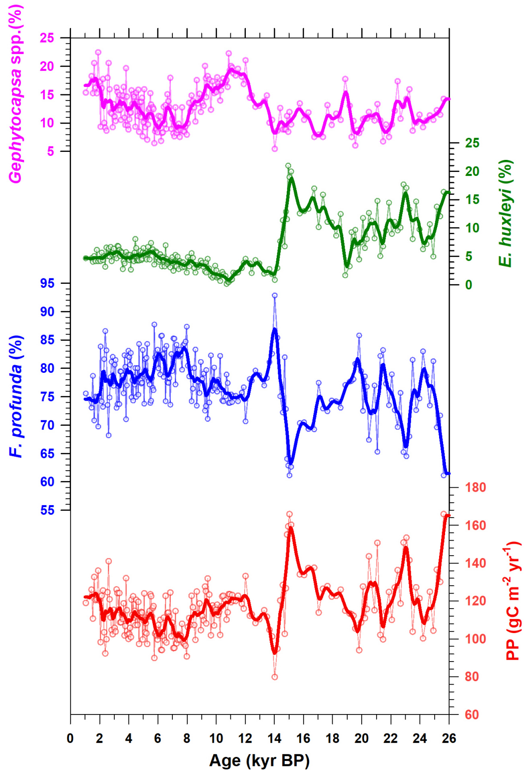

Fig. AC1. Relative abundance changes of main coccolith species and reconstructed PP.

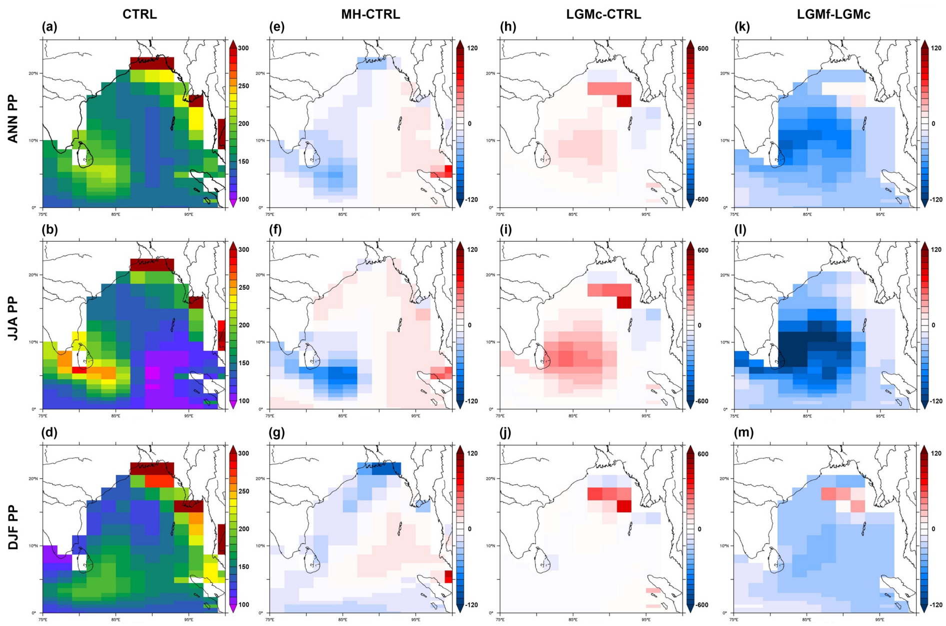

Fig. AC2. Simulated PP of CTRL and PP differences between MH and CTRL, LGMc and CTRL, and LGMf and LGMc. Results of annual mean, JJA mean and DJF mean are shown. PP is in gC m^{-2} yr^{-1}.

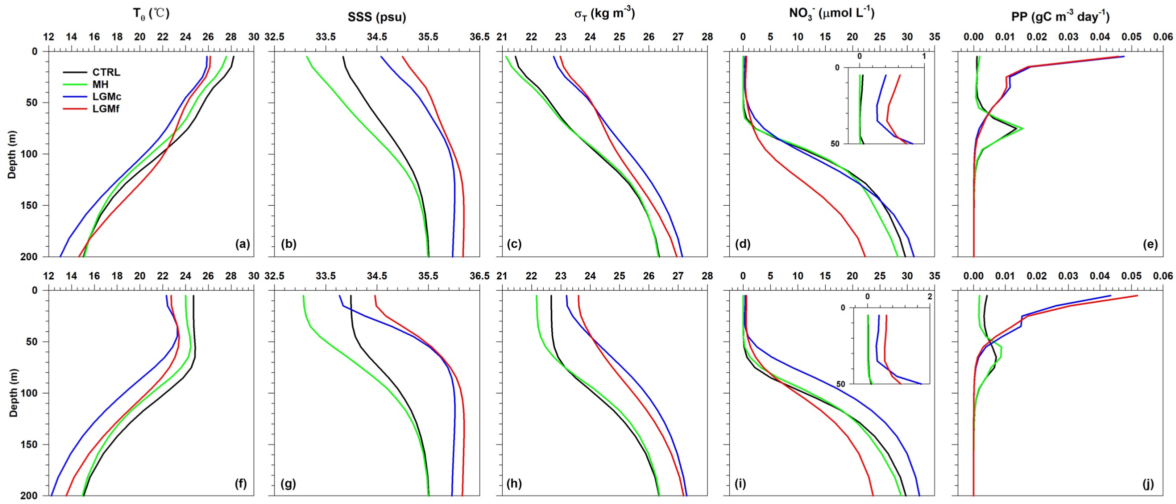

Fig. AC3. Simulated ocean profiles in four experiment run with IPSL-CM5A-LR. (a)–(e) Results of JJA mean. (f)–(j) Results of DJF mean. Grid of data extracting see Fig. S2. The parameters shown here are potential temperature (T_θ), sea surface salinity (SSS), potential density (sigma-t, σ_T), nitrate content of seawater (NO_3^-) and total primary productivity (PP).

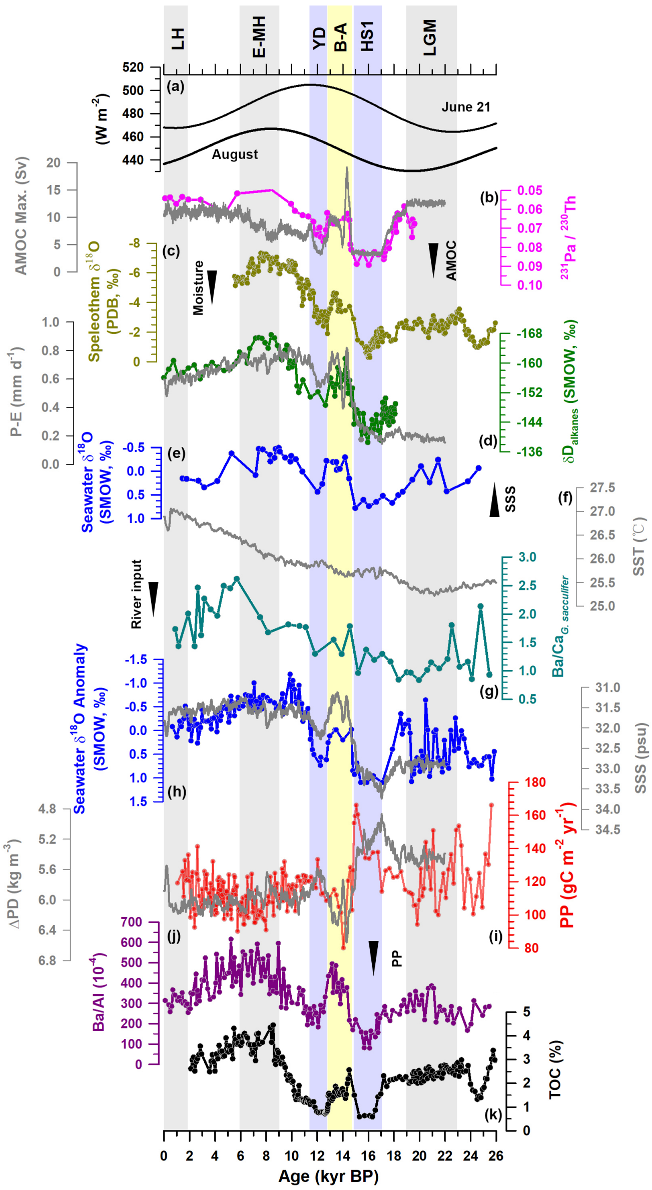

Fig. AC4. (a) August mean insolation and at 25°N. (b) AMOC strength indicated by $^{231}Pa/^{230}Th$ ratio of marine sediment from the western subtropical Atlantic Ocean (in pink, McManus et al., 2004). The changes of the maximum in the AMOC stream function below 500 m (AMOC strength) in TraCE-21 (in gray). (c) Mawmluh Cave speleothem $\delta^{18}O$ (Dutt et al., 2015). (d) Alkane δD in marine sediment, core SO188-342 (in green, Contreras-Rosales et al., 2014) and simulated precipitation minus evaporation of TraCE-21 (in gray). (e) Seawater $\delta^{18}O$ record of core RC12-344 (Rashid et al., 2007). (f) Simulated SST in the NE-BoB. Grids of data extracted see Fig. S2. (g) Ba/Ca ratios derived from mixed layer foraminifer species Globigerinoides sacculifer from core SK 168/GC-1(Gebregiogis et al., 2016). (h) Seawater $\delta^{18}O$ anomaly record of core MD77-176 (Marzin et al., 2013). (i) Estimated PP record of core MD77-176 (this study, in red) and simulated potential density gradient between 200 and 5m of TraCE-21 (in gray). (i) Ba/Al ratio of marine sediment, core 905 (Ivanochko et al., 2005). (j)

Total organic carbon weight percentage of marine sediment, core SO90-136KL (Schulz et al., 1998). Core locations of all these records above are marked in Fig. 1a. TraCE curves are shown using 100-yr averaged results.

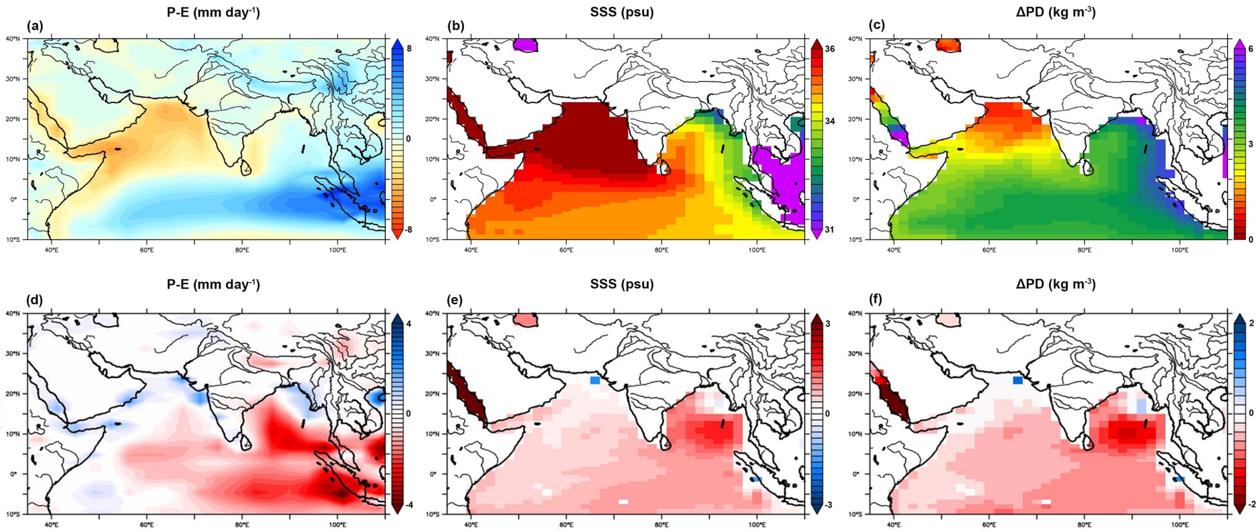

Fig. AC5. (a)–(c) Annual mean precipitation minus evaporation (P-E), sea surface salinity (SSS) and potential density gradient between 200 and 5 m of CTRL. (d)–(f) Differences of the same parameters between LGMc and CTRL.

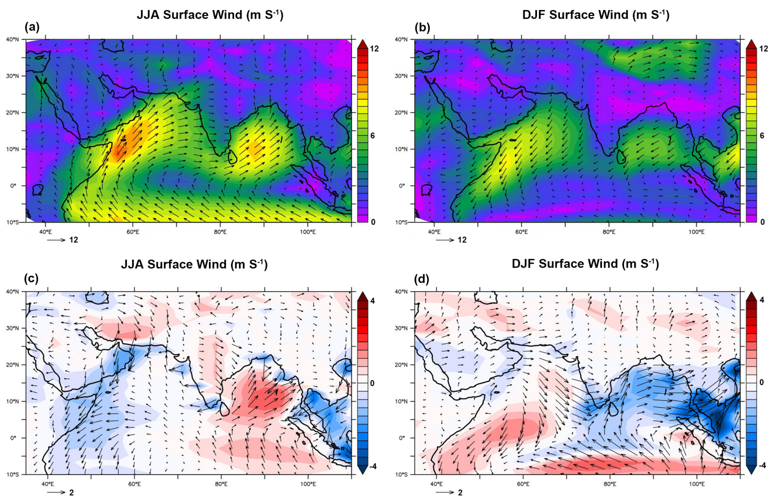

Fig. AC6. (a) and (b) JJA and DJF mean surface wind speed and vectors of CTRL. (c) and (d) Differences of the same parameters between LGMc and CTRL.

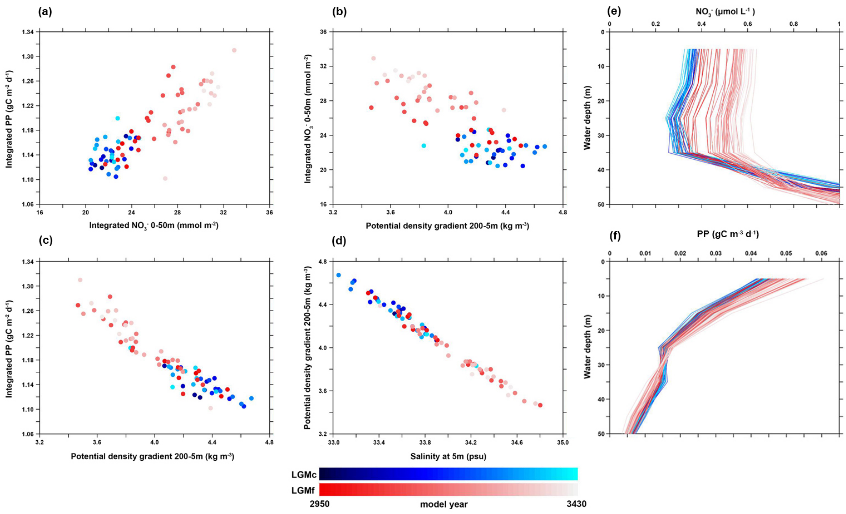

Fig. AC7. (a)–(d) Crossplots between different oceanic parameters of LGMc and LGMf (grids of data extracted see Fig. AC11). (e) and (f) Vertical profiles of nitrate content and PP of LGMc and LGMf (grids of data extracted see Fig. AC11). All the results are DJF mean and every curve represents an average of ten model years.

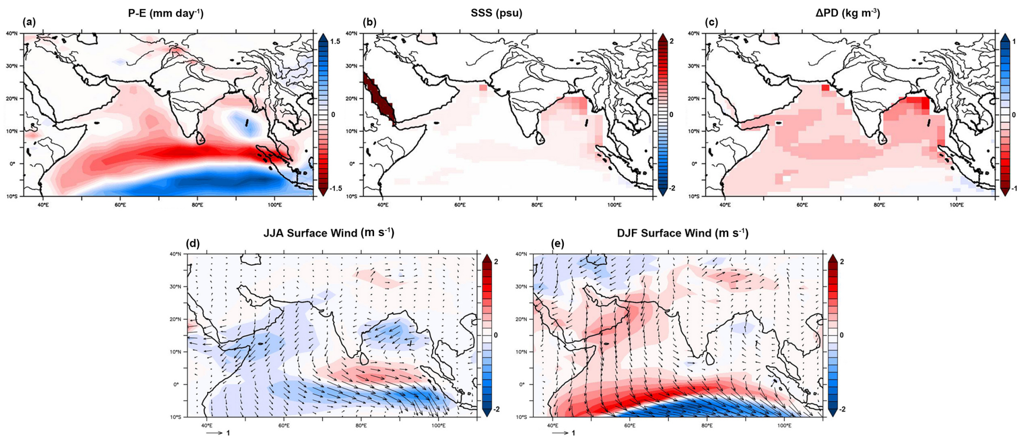

Fig. AC8. As in Fig. AC5 (d)–(f) and Fig. AC6 (c) and (d), but between LGMf and LGMc.

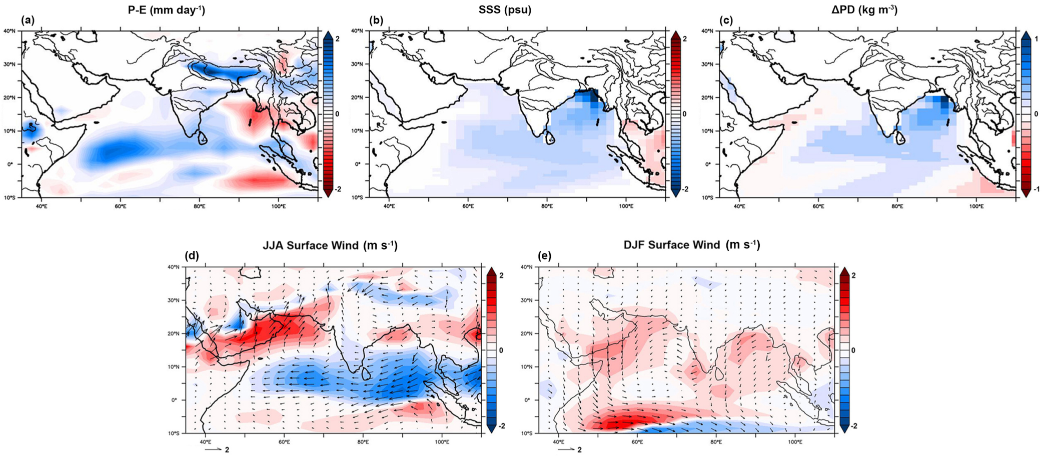

Fig. AC9. As in Fig. AC5 (d)–(f) and Fig. AC6 (c) and (d), but between MH and CTRL.

Supplementary Figures

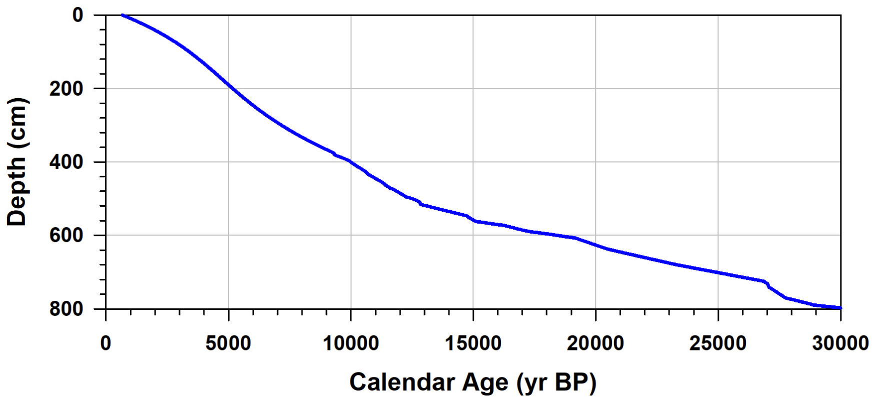

Fig. AC10. Tuned age model of MD77-176. The age model used in this studied is a tuned model constructed by Marzin et al., 2013. Details can be found in that article.

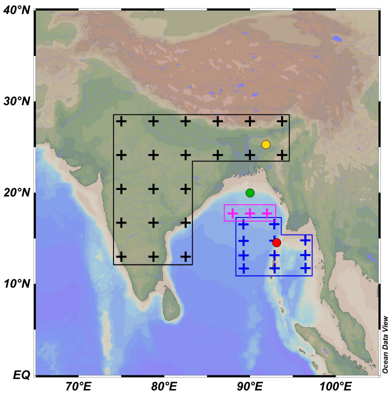

Fig. AC11. The grids of data extracting. Black cross are grids for TraCE-21 atmospheric outputs. Blue grids are for TraCE-21 oceanic outputs. Pink cross are grids for IPSL-CM5A-LR oceanic and biogeochemical outputs

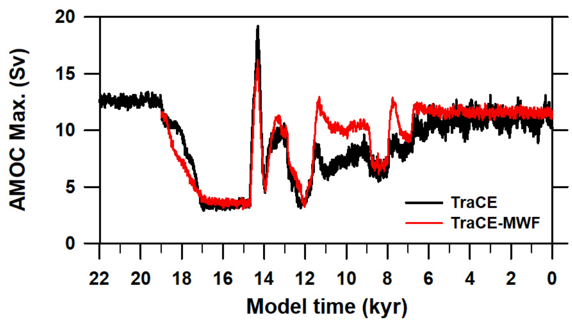

Fig. AC12. Changes of the maximum in the AMOC stream function below 500 m (AMOC strength) in TraCE and melt water of ice sheets single forcing simulation (MWF).

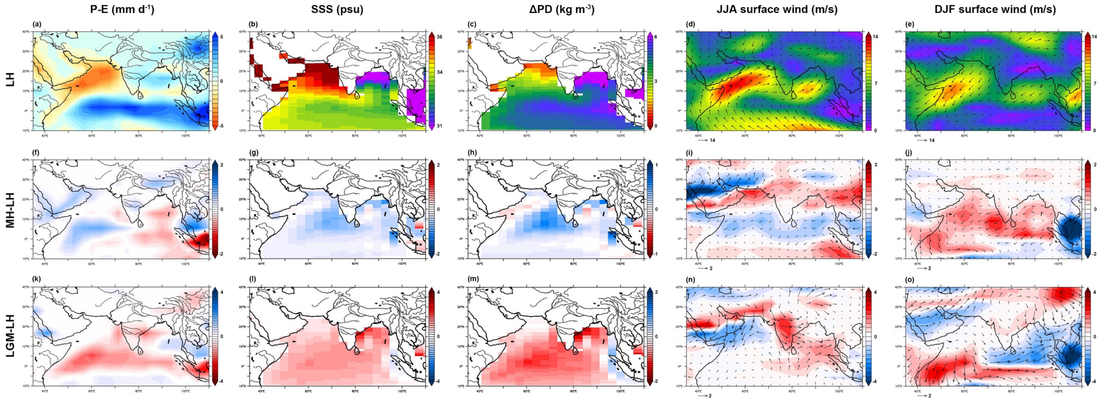

Fig. AC13. Results of TraCE-21 of three periods mean are shown: late Holocene (LH, from 1 kyr BP to presen), middle Holocene (MH, from 6.5 to 5.5 kyr BP), and the Last Glacial Maximum (LGM, from 23 to 19 kyr BP). (a)–(e) Annual mean precipitation minus evaporation (P-E), sea surface salinity (SSS) and potential density gradient between 200 and 5 m, JJA mean and DJF mean surface wind of LH. (f)–(j) Differences of the same parameters between MH and LH. (k) –(o) Differences of the same parameters between LGM and LH.

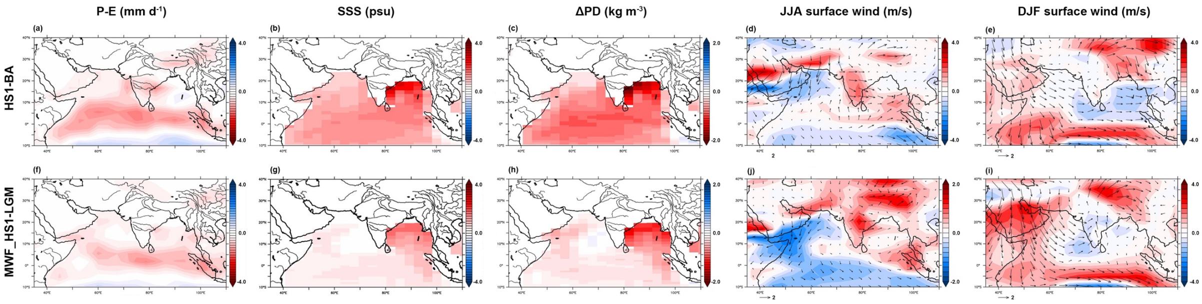

Fig. AC14. Results of TraCE-21 of three periods mean are shown: Bølling-Allerød (BA, from 14.5 to 13 kyr BP), and Heinrich Stadial 1 (HS1, from 17 to 15.5 kyr BP), and the Last Glacial Maximum (LGM, from 23 to 19 kyr BP). (a)–(e) As in Fig. AC13 (f)–(j), but between between BA and HS1. (f)–(j) As in Fig. AC13 (f)–(j), but between HS1 (melt water single forcing simulation) and LGM (full simulation). We can see the results are similar to the differences of the same parameters between LGMf and LGMc (see Fig. AC5, AC6).

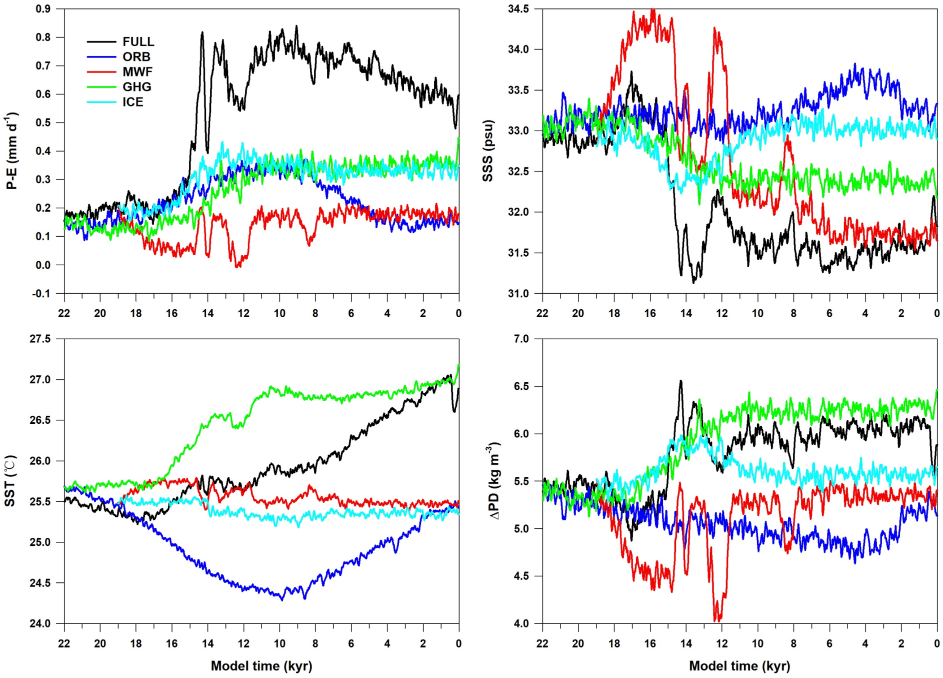

Fig. AC15. Annual mean results of precipitation minus evaporation, SSS, SST and potential density difference between 200 and 5 m (ΔPD) in TraCE-21 simulation (FULL) and single forcing experiments. The single forcing experiments are with other forcing fixed at their values at 19 kyr BP and forced by changing orbital insolation (ORB), green-house gas concentration (GHG), meltwater flux (MWF) and ice sheet (ICE). During the last deglaciation from 19 to 11 kyr BP, we can see that the millennial-scale variations of these parameters are mainly contributed by MWF forcing which moderated AMOC strength. The changes of SST during the deglaciation is very limited.